ACS Catalysis

pubs.acs.org/acscatalysis Research Article

Ferrocene-Functionalized Polyoxo-Titanium Cluster for CO_2 Photoreduction

Jing-Jing Liu, Ning Li, Jia-Wei Sun, Jiang Liu,* Long-Zhang Dong, Su-Juan Yao, Lei Zhang, Zhi-Feng Xin, Jing-Wen Shi, Jing-Xuan Wang, Shun-Li Li,* and Ya-Qian Lan*

Cite This: *ACS Catal.* 2021, 11, 4510−4519 Read Online

ACCESS | Metrics & More | Article Recommendations | Supporting Information

ABSTRACT: It is well-known that effective charge transfer within the catalyst structure is critical to the improvement of the performance of catalytic reaction. Herein, we reported three functionalized polyoxo-titanium clusters (PTCs)-based photocatalysts applied for photocatalytic CO_2 reduction reaction (CO_2RR): **Ti_6** functionalized with phenylphosphonic acid (PPOA), **Ti_8−Fcdc** and **Ti_6−Fcdc** functionalized with 1,1-ferrocene dicarboxylic acid (Fcdc). Notably, the light absorption range of **Ti_8−Fcdc** and **Ti_6−Fcdc** can be significantly expanded to the visible region, because the introduction of the Fcdc ligand with the ability to quickly transfer electrons triggers the intense electron transfer effect between Ti-oxo nucleus and Fcdc ligands. On this foundation, these three PTCs are demonstrated to be molecular photocatalysts to conduct visible light-driven photocatalytic CO_2RR in water with triisopropanolamine (TIPA) as holes scavenger. In particular, both of the Fcdc-functionalized **Ti_8−Fcdc** and **Ti_6−Fcdc** can accomplish the CO_2-to-$HCOO^-$ photoreduction in water with very high selectivity (96.2% and 97.5%, respectively) and activity (170.30 and 350.00 μmol g^{-1} h^{-1}, respectively). Most importantly, the photosynthetic of CO_2-to-$HCOO^-$ activity for **Ti_6−Fcdc** is the highest among the reported PTC photocatalytic for CO_2RR. Our work proves that the introduction of Fc-derived ligands can enhance the charge transfer efficiency of functionalized photocatalysts, thereby significantly affecting the photocatalytic performance of CO_2RR.

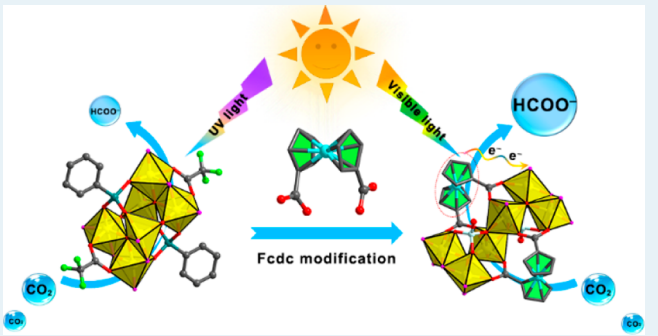

KEYWORDS: *polyoxo-titanium clusters, 1,1-ferrocene dicarboxylic acid, effective charge transfer, photocatalytic CO_2 reduction, high activity*

INTRODUCTION

In the past few decades, the continuous excessive emission of greenhouse gases mainly composed of CO_2 has caused serious environmental concerns, which need to be addressed.[1−6] The photocatalytic CO_2 reduction reaction (CO_2RR) has developed into a valuable and sustainable CO_2 conversion pathway, as it can use renewable solar energy to selectively reduce CO_2 to carbon-based energy products and reuse them.[7−16] However, given the chemical inertness and slow reaction kinetics of CO_2 molecules, its conversion process is extremely difficult.[17−20] Accordingly, the development of photocatalysts with high efficiency, low cost, strong photosensitivity and low toxicity (environmentally friendly) is of great significance for photocatalytic CO_2RR.[21−24]

It is well-known that TiO_2 as one of the most extensively used photocatalytic materials that has been widely used in many photocatalytic fields, such as degradation of photocatalytic dyes and pollutants, photocatalytic CO_2RR, and photocatalytic hydrogen production,[25−27] because of its prominent features including high stability, simple composition, low cost, easy synthesis, and nontoxicity. In order to further exploit the photocatalytic advantages of Ti-based materials, polyoxo-titanium clusters (PTCs) have a very similar structural composition as TiO_2, it has received extensive attention and research in recent years.[28−30] PTCs not only inherit the similar catalytic activity, low cost, and lower pollution of TiO_2, but also easily grow into a single crystal for structure identification.[31,32] Moreover, its clearly defined structural information is essential to establish an efficient structure−property relationship at the molecular level.[33,34] Recently, many research groups have made important progress in the synthesis and photocatalytic performance of PTCs. For instance, photocatalysis of hydrogen production, dye degradation, and CO_2RR.[35−38] Whereas, the application of Ti-based materials in photocatalytic CO_2RR is still rare. Only a few Ti-

Received: October 18, 2020
Revised: March 13, 2021

https://doi.org/10.1021/acscatal.0c04495
ACS Catal. 2021, 11, 4510−4519

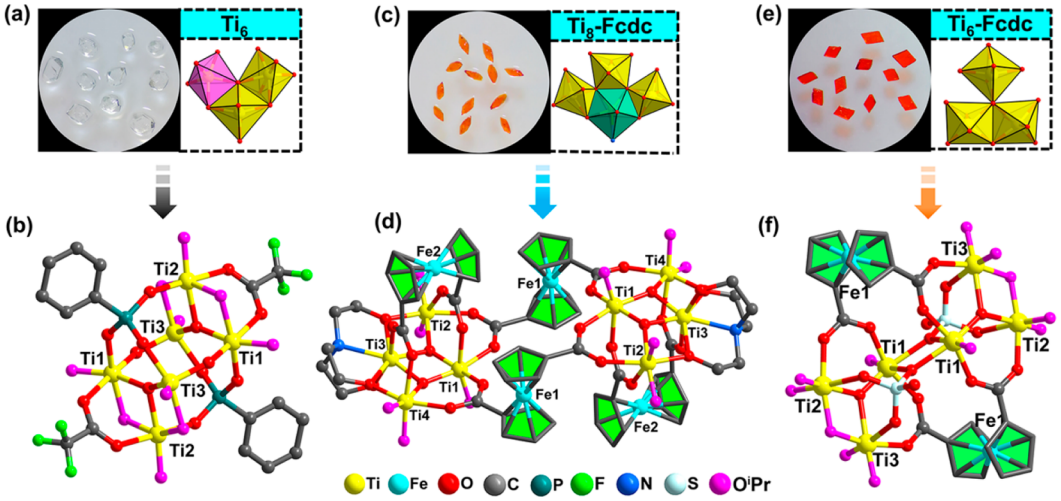

Figure 1. (a) The morphology and color of **Ti_6**; insets are the $Ti_3(\mu_3\text{-}O)$ unit of **Ti_6**. (b) The molecular structure view of **Ti_6**. (c) The morphology and color of **Ti_8−Fcdc**; insets are the edge-sharing $Ti_3(\mu_3\text{-}O)$ unit of **Ti_8−Fcdc**. (d) The molecular structure view of **Ti_8−Fcdc**. (e) The morphology and color of **Ti_6−Fcdc**; insets are the $Ti_3(\mu_3\text{-}O)$ unit of **Ti_6−Fcdc**. (f) The molecular structure view of **Ti_6−Fcdc**.

based MOFs and clusters (our previous works) have been reported for photocatalytic CO_2RR.[37−39] Among them, our group recently synthesized two PTCs PTi_{16} and PTi_{12} centered on phosphate (PO_4^{3-}), which are both classical Ti^{IV}-based heteroatom Keggin-type polyoxometalates and can act as high-efficiency photocatalysts to convert CO_2-to-$HCOO^-$ with highly selectivity under ultraviolet light.[38] Therefore, more attention should be paid to the synthesis of more novel PTCs for photocatalytic CO_2RR. Nevertheless, there are still many challenges in the application of traditional PTCs in photocatalytic applications. The most important deficiency is that their band gaps are usually wide (only ultraviolet light response), which makes the catalyst materials unable to utilize longer wavelength sunlight spectra such as visible light and near-infrared light. To effectively solve this problem, the band gap of traditional PTCs is mainly regulated by ligand modification to change their light absorption range, thereby reducing the band gap.[40−42] In addition, effectively regulating the photogenerated electron-transfer rate within the crystalline molecular photocatalyst should be crucial to improve the catalytic performance, but there are still no reports in the field of photocatalytic CO_2RR. Consequently, it is necessary to select appropriate functionalized organic ligands to construct novel PTCs that have an expanded light absorption range and excellent photogenerated charge migration rate to enhance the performance of photocatalytic CO_2RR.

Ferrocene (Fc)-modified complexes usually exhibit diverse structure types, extended light absorption, and fast charge-transfer rates, so they have been applied as efficient and stable electron donors in many optoelectronic applications.[43,44] However, to the best of our knowledge, only a few PTCs with Fc-derived functional ligands have been reported to date, and these PTCs also exhibit similar photocurrent responses and significant band gap reduction.[45−48] On the basis of these results, we hope to effectively regulate the structural composition, light absorption, and charge transfer efficiency of PTCs by introducing Fc-based organic ligands into traditional PTCs, and then improve the corresponding photocatalytic performance of CO_2RR. Herein, $[Ti_6(\mu_3\text{-}O)_2(\mu_2\text{-}O)_2(PPO)_2(O_2CCF_3)_2(\mu_2\text{-}O^iPr)_4(O^iPr)_6]$ (CF_3COOH = trifluoroacetic acid, HO^iPr = isopropanol, **Ti_6**) and Fcdc-functionalized $[Ti_8(\mu_3\text{-}O)_4(tea)_2((Fcdc)_2)_4(O^iPr)_{10}]\cdot 2HO^iPr$ ($teaH_3$ = Triethanolamine, **Ti_8−Fcdc**) and $[Ti_6(\mu_3\text{-}O)_2(Fcdc)_2(\mu_2\text{-}SO_4)_2(\mu_2\text{-}O^iPr)_2(O^iPr)_{10}]\cdot 2HO^iPr$ (**Ti_6−Fcdc**) are successfully synthesized by solvent thermal methods. Among them, **Ti_6** has been reported in previous work.[42] The crystal structure, spectroscopic properties, and photoelectrochemical properties of these three PTCs are studied, we found that the light absorption range of **Ti_8−Fcdc** and **Ti_6−Fcdc** with Fcdc ligand modification extends to the visible region, and the photocurrent response is correspondingly improved (effective photogenerated charge transfer rate), compared with **Ti_6**, in which Fcdc ligand is not involved. Taking these advantages into consideration, we further conducted research on the photocatalytic CO_2RR under visible light for the three PTCs, respectively. Photocatalytic CO_2RR results showed that three PTCs can accomplish CO_2-to-$HCOO^-$ conversion with high selectivity. **Fcdc** functionalized **Ti_8−Fcdc** and **Ti_6−Fcdc** revealed higher photocatalytic activity and selectivity compared with **Ti_6**. Our work represents an important case study for the development of photosensitive and higher photogenerated charge transfer efficiency PTCs for artificial photoreduction of CO_2.

EXPERIMENTAL SECTION

Syntheses of Ti_6. A mixture of PPOA (47.4 mg, 0.3 mmol) and CF_3COOH (0.03 mL, 0.55 mmol) was dispersed in isopropanol (5 mL) with stirring for about 10 min. After addition of Ti $(O^iPr)_4$ (0.315 mL, 1 mmol), a clear colorless solution was formed. The resultant mixture was heated at 100 °C for 3 days in a Teflon-lined autoclave. After being cooled to room temperature, colorless cubic block crystals were obtained by filtration and were fully washed several times with isopropanol. Yield: ca. 70%.

Syntheses of Ti_8−Fcdc. A mixture of Fcdc (27.4 mg, 0.1 mmol) and $teaH_3$ (0.3 mL, 2.26 mmol) dispersed in isopropanol (1 mL) with stirring for about 10 min. After addition of $Ti(O^iPr)_4$ (0.945 mL, 3 mmol), a clear deep-red solution was formed. The resultant mixture was heated at 80 °C for 3 days in a Teflon-lined autoclave. After being cooled to room temperature, yellow rhombic block crystals were

https://doi.org/10.1021/acscatal.0c04495
ACS Catal. 2021, 11, 4510−4519

obtained by filtration and were fully washed several times with isopropanol. Yield: ca. 80%.

Syntheses of Ti_6−Fcdc. A mixture of Fcdc (27.4 mg, 0.1 mmol) and sulfuric acid (0.05 mL, 0.933 mmol) was dispersed in isopropanol (5 mL) with stirring for about 10 min. After addition of $Ti(O^iPr)_4$ (0.470 mL, 1.5 mmol), a clear deep-red solution was formed. The resultant mixture was heated at 80 °C for 3 days in a Teflon-lined autoclave. After being cooled to room temperature, red rhombic block crystals were obtained by filtration and were fully washed several times with isopropanol. Yield: ca. 72%.

RESULTS AND DISCUSSION

Ti_6, **Ti_8−Fcdc**, and **Ti_6−Fcdc** are synthesized by in situ solvent thermal synthesis (see the Experimental Section) with relatively high yields. As shown in Figures 1 and S2 of the Supporting Information (SI), **Ti_6**, **Ti_8−Fcdc**, and **Ti_6−Fcdc** appear as colorless cubic, yellow rhombic, and red rhombic block crystals under the optical microscope, respectively. These three different PTCs are constructed using oxygen centered $Ti_3(\mu_3\text{-}O)$ unit and different bridging ligands (including CF_3COOH, PPOA, $teaH_3$, Fcdc, and H_2SO_4). Among them, **Ti_6** mainly contains two planar triangle $Ti_3(\mu_3\text{-}O)$ units connected by two μ_2-O, two PPOA, and two CF_3COOH (Figure S3). **Ti_8−Fcdc** is an octa-nuclear cluster consists of two Ti_4 motifs (each Ti_4 motif involves two edge-sharing $Ti_3(\mu_3\text{-}O)$ units) connected by two Fcdc ligands (Figure S4). **Ti_6−Fcdc** is a hexa-nuclear PTC that constructed from two $Ti_3(\mu_3\text{-}O)$ units bridged by two Fcdc and SO_4^{2-} ligands (Figure S5).

X-ray single crystal diffraction analysis demonstrates that the space group of the **Ti_6** cluster is $P2_1/n$, and its asymmetric unit involves three Ti atoms (Ti1, Ti2, Ti3), two μ_3-O atoms, one CF_3COOH, one PPOA, and five -O^{i}Pr groups (Figure S6a). The hexa-nuclear molecular structure of **Ti_6** is built by two triangle-shaped $Ti_3(\mu_3\text{-}O)$ units connected with two couples of μ_2-O and PPOA ligand (Figure S6b). It is worth noting that the six-coordinated Ti1 and Ti2 atoms exhibit slightly distorted octahedral geometry, while the five-coordinated Ti3 atom shows distorted tetragonal pyramid geometry (Figure S6c). The Ti1 and Ti2 atoms in the $Ti_3(\mu_3\text{-}O)$ unit are coordinated with a CF_3COOH (Figure S9a). The three O atoms of PPOA are respectively connected with Ti1 and Ti3 atoms in $Ti_3(\mu_3\text{-}O)$ unit and Ti2 atom in another $Ti_3(\mu_3\text{-}O)$ unit (Figure S9b). The outer coordination space of **Ti_6** is surrounded by 10 isopropyl groups, in which four isopropyl groups are used to bridge two neighboring Ti atoms and the others are all terminal ligands.

To change the light absorption range of PTC and enhance the electron transfer efficiency between the ligand and the titanium oxide core, we have replaced the PPOA and CF_3COOH ligands with Fcdc ligands, and obtained two PTCs **Ti_8−Fcdc** and **Ti_6−Fcdc** with Fcdc functionalized. **Ti_8−Fcdc** has the identical space group as **Ti_6** (Table S1a). As illustrated in Figure S7a, the asymmetric unit of **Ti_8−Fcdc** contains four Ti atoms, two μ_3-O atoms, one $teaH_3$, two Fcdc ligands, five -O^{i}Pr groups, and a free HO^{i}Pr molecule. Similar to **Ti_6**, the structure of **Ti_8−Fcdc** also includes two kinds of planar triangle $Ti_3(\mu_3\text{-}O)$ unit with μ_3-O atom connected with Ti1, Ti2, and Ti3 atoms or Ti1, Ti3, and Ti4 atoms. Moreover, these two $Ti_3(\mu_3\text{-}O)$ units further form an edge-sharing $Ti_4(\mu_3\text{-}O)_2$ unit, and the $Ti_4(\mu_3\text{-}O)_2$ unit is coordinated with a $teaH_3$ and a Fcdc ligand, at the same time, it is further bridged by two Fcdc to form an octa-nuclear cluster (Figure S7b). Six-coordinated Ti1, Ti2, and Ti4 atoms in **Ti_8−Fcdc** possess the slightly distorted octahedral geometry configuration, while the seven-coordinated Ti3 atom shows a pentagonal bipyramid coordination environment (Figure S7c). Importantly, the Fcdc ligand can serve as a potential electron transport channel, which can effectively increase the charge transfer between two $Ti_4(\mu_3\text{-}O)_2$ units in **Ti_8−Fcdc**. Furthermore, three O atoms and one N atom of $teaH_3$ are coordinated with Ti2, Ti3, and Ti4 atoms (Figure S9c). The four O atoms of Fcdc ligand (Fe1) respectively connected with Ti1, Ti2 atoms in $Ti_4(\mu_3\text{-}O)_2$ unit, and Ti1 and Ti3 atoms in another $Ti_4(\mu_3\text{-}O)_2$ unit (Figure S9d), while the four O atoms of another Fcdc ligand (Fe2) coordinate with Ti1, Ti2, Ti3, and Ti4 atoms in a $Ti_4(\mu_3\text{-}O)_2$ unit, respectively (Figure S9e). Ti1, Ti2, and Ti4 atoms of **Ti_8−Fcdc** are coordinated with easily detachable -O^{i}Pr groups in the axial position.

In contrast to **Ti_6** and **Ti_8−Fcdc**, the space group of the **Ti_6−Fcdc** crystal is $C2/c$ with relatively high symmetry (Table S1a). As illustrated in Figure S8a, the asymmetric unit of the **Ti_6−Fcdc** contains three independent Ti atoms, one μ_3-O atom, one Fcdc, one sulfate radical, and six -O^{i}Pr groups is composed of a free HO^{i}Pr molecule. In the structure of **Ti_6−Fcdc**, Ti1, Ti2, and Ti3 atoms are also linked with a μ_3-O atom to construct a planar triangle $Ti_3(\mu_3\text{-}O)$ unit, two $Ti_3(\mu_3\text{-}O)$ units are bridged via two Fcdc and two sulfate anions to form a hexa-nuclear cluster (Figure S8b). Notably, the six Ti atoms within the **Ti_6−Fcdc** structure are six-coordinated, and all of them adopt distorted octahedral geometry (Figure S8c). Same as that in **Ti_8−Fcdc**, the linkage mode of Fcdc ligands in **Ti_6−Fcdc** also involves Ti1, Ti2 atoms in one planar triangle $Ti_3(\mu_3\text{-}O)$ unit and Ti1, Ti3 atoms in another $Ti_3(\mu_3\text{-}O)$ unit (Figure S9f). The Fcdc ligand in **Ti_6−Fcdc** can improve the charge transfer between the two $Ti_3(\mu_3\text{-}O)$ units, which is more effective than **Ti_8−Fcdc** because of the shorter transmission distance. Additionally, there are also two SO_4^{2-} bridges that use its three O atoms to link with Ti1, Ti2, and Ti3 atoms in one $Ti_3(\mu_3\text{-}O)$ unit and Ti1 atom in another $Ti_3(\mu_3\text{-}O)$ unit, so that two couples of Ti1 atom and μ_2-SO_4 form a parallelogram plane (Figure S9g). More importantly, this parallelogram plane further shortens the distance between the two $Ti_3(\mu_3\text{-}O)$ units, forming two additional potential channels for electron transfer, thus achieving faster and more efficient electron transport. The outer surface of **Ti_6−Fcdc** is coordinated by 12 isopropyl molecules and two sulfate radicals. Two isopropyl groups are used as bridging ligands to link Ti2 and Ti3 atoms, and the others act as terminal ligands. Analogously, -O^{i}Pr groups coordinated to Ti1, Ti2, and Ti3 atoms in **Ti_6−Fcdc** easily leave to build open active metal sites.

The experimental powder X-ray diffraction (PXRD) patterns of **Ti_6**, **Ti_8−Fcdc**, and **Ti_6−Fcdc** are identical to the simulation results of crystallographic data, which indicates that they have high purity (Figures S10−S12). The thermogravimetric analysis (TGA) curves of **Ti_6**, **Ti_8−Fcdc**, and **Ti_6−Fcdc** show that their structures can be maintained up to about 230 °C, 200 °C, and 330 °C, respectively (Figure S13). The Infrared (IR) spectra of **Ti_6**, **Ti_8−Fcdc**, and **Ti_6−Fcdc** as displayed in Figure S14. The vibrations of Ti−O−C (between 1000 and 1003 cm^{-1}) as well as C−H (between 2990 and 2855 cm^{-1}) represent -O^{i}Pr groups. The frequency band 609 cm^{-1} belongs to the Ti−O vibration. The bands of ∼1480 cm^{-1} in **Ti_8−Fcdc** and **Ti_6−Fcdc** are designated as the characteristic bands of the Fc moiety.[49] The X-ray photo-

https://doi.org/10.1021/acscatal.0c04495
ACS Catal. 2021, 11, 4510−4519

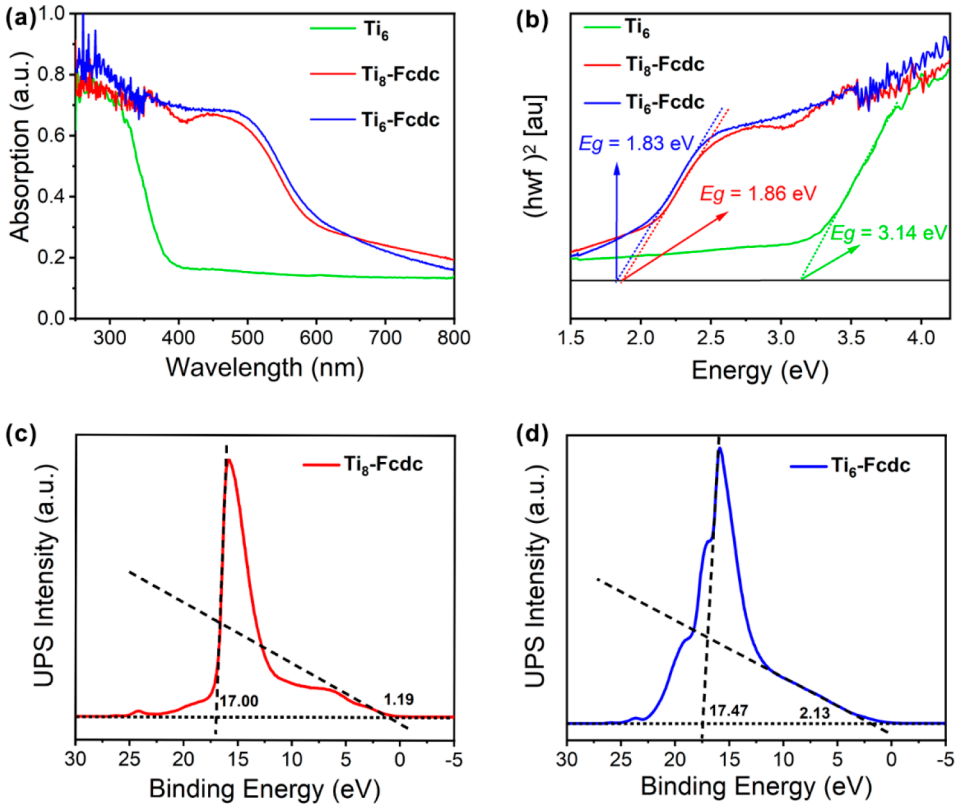

Figure 2. (a) Solid-state UV−vis absorption spectrum of **Ti_6**, **Ti_8−Fcdc**, and **Ti_6−Fcdc**. (b) $(hwf)^2$vs $h\nu$ curve of **Ti_6**, **Ti_8−Fcdc** and **Ti_6−Fcdc**. (c) UPS spectra of **Ti_8−Fcdc**. (d) UPS spectra of **Ti_6−Fcdc**.

electron spectroscopy (XPS) is characterized to identify the valence states of Ti and Fe atoms in **Ti_8−Fcdc** and **Ti_6−Fcdc** (Figures S15−S17). The Ti 2p spectrum of **Ti_6−Fcdc** exhibits that the peak at 458.8 eV is the state of Ti $2p_{2/3}$, while the peak at 464.6 eV refers to the state of Ti $2p_{1/2}$, indicating that only Ti^{4+} exists in **Ti_6−Fcdc** (Figure S15e). The high-resolution Fe 2p spectra of **Ti_6−Fcdc** clearly displays two peaks of 708.1 eV (Fe $2p_{2/3}$) and 720.8 eV (Fe $2p_{1/2}$) (Figure S15f), which indicates the unique existence of Fe^{2+} in **Ti_6−Fcdc**.[48,50]

It is well-known that the reported PTCs, as well as Ti-based MOFs or Ti-based nanomaterials have shown inherent photoactivity for widespread photocatalytic applications, in which light absorption capacity is an essential factor in deciding their photocatalytic performance.[39] Therefore, the solid-state UV−visible (UV−vis) absorption spectrum is used to evaluate the light absorption capacity of these PTCs and Fcdc ligand (Figure S18). As shown in Figure 2a, it is obvious that the UV−vis spectra of **Ti_6** exhibits a significant absorption around 330 nm, and there is a weak absorption (low absorbance) in the visible region (450 nm) (Figure S19). In contrast, the Fcdc-functionalized **Ti_8−Fcdc** and **Ti_6−Fcdc** exhibit strong absorption and wide absorption bands, with a maximum absorption of about 500 nm extending to about 600 nm. The excellent UV−visible absorption bands of **Ti_8−Fcdc** and **Ti_6−Fcdc** are mainly attributed to the high valence state of Ti^{4+} ions and the good electron donating ability of Fc groups, which obviously makes the charge transfer from Fcdc ligand to Ti^{4+} ion.[51] The optical band gap (E_g) of **Ti_6**, **Ti_8−Fcdc**, and **Ti_6−Fcdc** are further calculated using the **Kubelka−Munk** function, and are estimated to be 3.14 (**Ti_6**), 1.86 (**Ti_8−Fcdc**), and 1.83 eV (**Ti_6−Fcdc**) (Figure 2b).[52] Since the π conjugation is between the cyclopentadiene ring and the carboxylic acid bond in Fcdc ligands, the charge of Fc group is delocalized to the core of Ti-oxo cluster, which stabilizes the excited state, reduces the transition energy, enhances the charge transfer characteristics, greatly improves the absorption intensity, broadens the visible absorption band, and reduces the band gap significantly.[48] However, in the titanium-oxo core of **Ti_6**, the charge transition of O → Ti can only induce its ultraviolet absorption. In order to determine the HOMO position of these three PTCs, ultraviolet photoelectron spectroscopy (UPS) is performed (Figures 2c,d and S20). The final HOMO positions of **Ti_6**, **Ti_8−Fcdc** and **Ti_6−Fcdc** are calculated as 7.08 (2.23 V vs NHE), 5.41 (0.56 V vs NHE), and 5.88 eV (1.03 V vs NHE), respectively. The corresponding LUMO positions are calculated by $E_v - E_g$ to be 4.06 (**Ti_6**), 3.55 (**Ti_8−Fcdc**), and 4.06 eV (**Ti_6−Fcdc**), respectively. Subsequently, Mott−Schottky electrochemical measurements are performed to confirm the accuracy of the corresponding LUMO and HOMO energy levels of the prepared **Ti_6**, **Ti_8−Fcdc**, and **Ti_6−Fcdc**. The LUMO positions of these three PTCs are determined to be −0.90 (**Ti_6**), −1.30 (**Ti_8−Fcdc**), and −0.77 V (**Ti_6−Fcdc**) (vs NHE, pH = 7), respectively (Figures S21−S23). Therefore, the HOMO positions of the three PTCs are determined to be 2.24 (**Ti_6**), 0.56 (**Ti_8−Fcdc**), and 1.06 V (**Ti_6−Fcdc**) (vs NHE, pH = 7) respectively associated with solid-state UV−visible absorption spectrum. These results are consistent with UPS. Obviously, the LUMO energy levels of these three PTCs are very negative, therefore, they may become crystalline molecular photocatalysts for CO_2RR theoretically.

https://doi.org/10.1021/acscatal.0c04495
ACS Catal. 2021, 11, 4510−4519

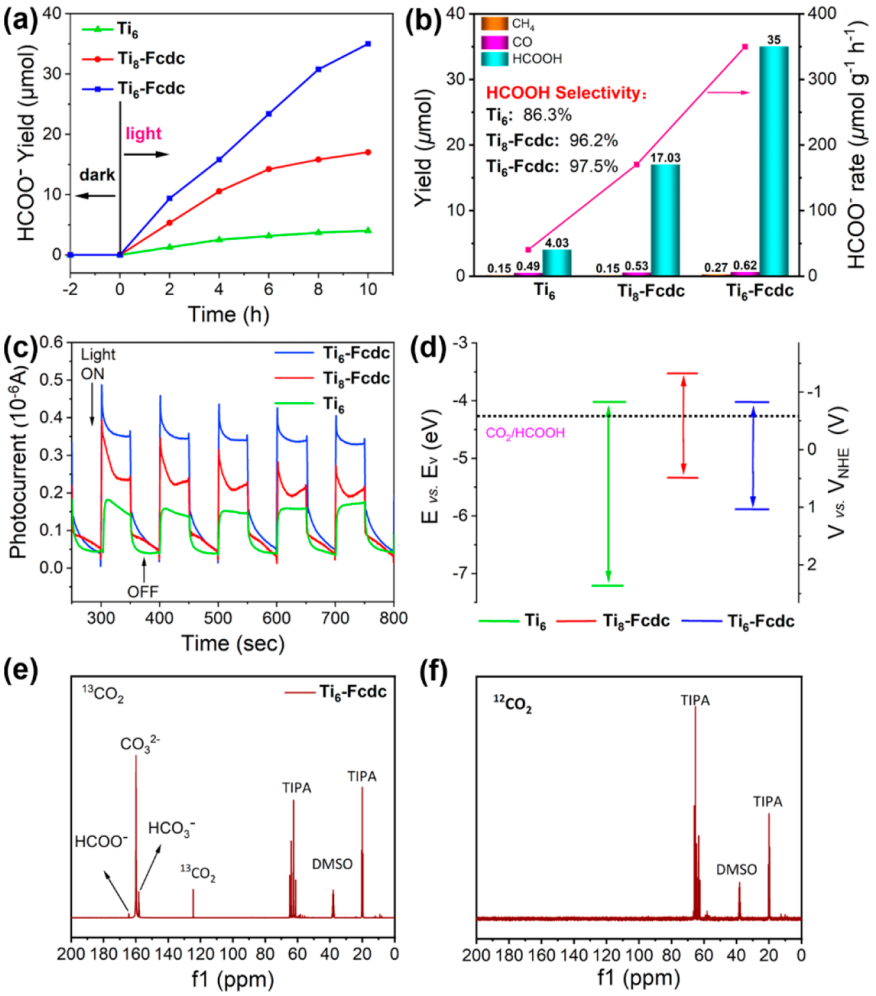

Figure 3. (a) The relationship between the yield of $HCOO^-$ and the irradiation time (visible light) on **Ti_6**, **Ti_8−Fcdc**, and **Ti_6−Fcdc**. (b) The selectivity of $HCOO^-$ and the yield distribution of different photoreduction products. (c) Transient photocurrent responses of **Ti_6**, **Ti_8−Fcdc**, and **Ti_6−Fcdc** under visible light irradiation. (d) The energy band structure diagram for **Ti_6**, **Ti_8−Fcdc**, and **Ti_6−Fcdc**. (e) The ^{13}C NMR spectrum of the product obtained by adding $^{13}CO_2$ into the reaction of **Ti_6−Fcdc**. (f) The ^{13}C NMR spectrum for the product obtained by adding $^{12}CO_2$ into the reaction of **Ti_6−Fcdc**.

On the basis of the above advantages, the photocatalytic CO_2RR over **Ti_6**, **Ti_8−Fcdc**, and **Ti_6−Fcdc** is performed under visible light, with H_2O and TIPA as the reaction solvent and electron donor, respectively, and without any photosensitizers and noble metal promoters. By testing the $HCOO^-$ yields at 2, 4, 6, 8, and 10 h, respectively, we obtained the function between $HCOO^-$ yield and the irradiation time. As shown in Figure 3a, $HCOO^-$ production of these three PTCs increased continuously with the increase of irradiation time within 10 h. What's more, the yields of CO_2-to-$HCOO^-$ reduced by **Ti_6**, **Ti_8−Fcdc**, and **Ti_6−Fcdc** grew to 4.03, 17.03, and 35.00 μmol in 10 h. From a structural point of view, we assumed that there are six Ti atoms as potential active centers in **Ti_6**, **Ti_8−Fcdc** and **Ti_6−Fcdc**. Therefore, the catalytic performances of the active centers in **Ti_6**, **Ti_8−Fcdc**, and **Ti_6−Fcdc** are calculated and compared according to the parameters including turnover number (TON) and turnover frequency (TOF).[53] As indicated in Table S2, the TON_{Ti} of Ti^{4+} catalytic sites in **Ti_8−Fcdc** and **Ti_6−Fcdc** are 27.12 and 39.60, respectively, which are more active than **Ti_6**. Thus, the higher photocatalytic performance of **Ti_8−Fcdc** and **Ti_6−Fcdc** compared with that of **Ti_6** is mainly due to their modification with Fcdc ligands that have the ability to quickly transfer charges. Until now, only two cases of PTCs (our previous work) have been reported for photocatalytic CO_2RR.[37,38] Moreover, they mainly reduce CO_2-to-$HCOO^-$ with high activity under ultraviolet irradiation and exhibit relatively low photocatalytic performance under visible light. Fcdc functionalized **Ti_8−Fcdc** and **Ti_6−Fcdc** in this work show higher photocatalytic CO_2-to-$HCOO^-$ activity compared with the PTCs reported. In this work, $HCOO^-$ is the only photocatalytic liquid product detected by ion chromatography (IC; Figure S24), whereas traces of gaseous CO and CH_4 byproducts are tested by gas chromatography (GC) during the photoreaction process (Figures S25a, S26a, and S27a), what's more, there is no subsidiary H_2 produced during the entire reaction (Figures S25b, S26b, and S27b). It is noteworthy that the yields of CO_2-to-$HCOO^-$ reduced by **Ti_8−Fcdc** and **Ti_6−Fcdc** under visible light are 17.03 μmol (170.30 μmol g^{-1} h^{-1}) and 35.00 μmol (350.00 μmol g^{-1} h^{-1}), which are significantly superior to the $HCOO^-$ production of **Ti_6** (4.03 μmol; corresponding to 40.30 μmol g^{-1} h^{-1}) (Figure 3b). According to the distribution of reduction products, it is obvious that these PTCs show higher photocatalytic selectivity for CO_2RR. The selectivity of **Ti_6**, **Ti_8−Fcdc** and **Ti_6−Fcdc** is

https://doi.org/10.1021/acscatal.0c04495
ACS Catal. 2021, 11, 4510−4519

86.3%, 96.2%, and 97.5%, respectively. Compared with **Ti_6**, Fcdc-functionalized **Ti_8−Fcdc** and **Ti_6−Fcdc** show higher photocatalytic activity and selectivity for photocatalytic CO_2RR, it is ascribed to the quick transfer of photogenerated charges by the Fcdc ligand. As the bridged sulfate radical may provide additional electron transport channels along with increasing the effective charge transfer, the photocatalytic CO_2RR performance of **Ti_6−Fcdc** is significantly higher than that of **Ti_8−Fcdc**. The photoactivity difference (charge separation efficiency) of these PTC-based photocatalysts is demonstrated by many measurement techniques. The transient short-circuit photocurrent response test is carried out to explore the efficiency of photoinduced electron transfer. The anode photocurrent responses of **Ti_6**, **Ti_8−Fcdc**, and **Ti_6−Fcdc** indicated that these PTCs behave as n-type semiconductors (Figure 3c). The photocurrent is generated quickly when the visible light is turned on, and then remains stable with no significant intensity reduction. While the visible light is turned off, the photocurrent decays rapidly, which reveals that the three PTCs all have a good photocurrent response. Notably, the Fcdc functionalized **Ti_8−Fcdc** and **Ti_6−Fcdc** photoelectrodes showed significantly enhanced photocurrent response by comparing it with **Ti_6**, indicating that the excited state of the Fcdc ligand is more effective in injecting electrons, resulting in better electron-coupling between the Fcdc ligand and PTCs core.[46,54] It is noteworthy that the **Ti_6−Fcdc** exhibits a relatively higher photocurrent response than **Ti_8−Fcdc**, which is attributed to sulfate radical as a bridging ligand to provide additional electronic transmission channels. The good separation of photoinduced electrons and holes in the Fcdc functionalized **Ti_6−Fcdc** can increase the surface photoinduced electron density of the photocatalyst, thus the rate of multielectron reduction reaction is accelerated dynamically to making the reduction products display higher selectivity.[55] Electrochemical impedance spectroscopy (EIS) test is performed to verify the charge separation efficiency (Figure S29). It can be seen from the Nernst spectra of these three PTCs that the impedance of **Ti_6−Fcdc** is significantly less than that of **Ti_6** and **Ti_8−Fcdc**, which indicates that the rate of surface charge transport of PTCs is **Ti_6−Fcdc** > **Ti_8−Fcdc** > **Ti_6**. Therefore, the charge separation efficiency of **Ti_6−Fcdc** is indeed the highest, which is also in agreement with the transient short-circuit photocurrent response. In addition, Photoluminescence (PL) (Figures S30−S32) and time-resolved fluorescence decay techniques (Figures S33−S35) are performed to further investigate the intramolecular charge transfer behavior of **Ti_6**, **Ti_8−Fcdc**, and **Ti_6−Fcdc**. The corresponding results are consistent with the transient short-circuit photocurrent response and EIS test data. Besides, different monochromatic lights (420/450/500 nm) are used to measure the apparent quantum efficiency (AQE) of $HCOO^-$ evolution (Table S4), and the results showed that **Ti_8−Fcdc** and **Ti_6−Fcdc** have higher AQE than **Ti_6** (Table S5). It is noteworthy that the Fcdc functionalized PTCs exhibit better photoreduction performance of CO_2 under visible light. What is demonstrated in Figure 3d is the band alignment results of the three PTCs. Obviously, the LUMO energy levels of **Ti_6**, **Ti_8−Fcdc**, and **Ti_6−Fcdc** is very negative, compared with oxidation−reduction potential of many photoreduction products such as $HCOO^-$ (−0.58 V vs NHE, pH 7), CO (−0.51 V vs NHE, pH 7), and CH_4 (−0.24 V vs NHE, pH 7), which further demonstrates that all three PTCs can reduce CO_2 to $HCOO^-$.

In addition, to confirm the photocatalytic activity of these PTCs, the carbon source of $HCOO^-$ is determined by isotope $^{13}CO_2$ experiments on Fcdc-functionalized **Ti_8−Fcdc** and **Ti_6−Fcdc** with the same photocatalytic reaction conditions. As illustrated in Figures 3e and S36, the ^{13}C NMR spectrum gives a clear signal at 164.5 ppm, which corresponds to $HCOO^-$. These signals are consistent with other important works of our group.[9,37,38,52] When $^{12}CO_2$ is introduced into the same reaction system, no additional signals are detected in the ^{13}C NMR except for the peaks of TIPA and deuterated DMSO (Figure 3f). Besides, the photocatalytic lifetime of the three PTC based photocatalysts was performed (Figure S37). To determine the photocatalytic activity of **Ti_6**, **Ti_8−Fcdc**, and **Ti_6−Fcdc**, a series of selective control experiments are carried out under no light irradiation, no catalyst, and in an Ar atmosphere. The results show that IC and GC did not detect the product (Table S6a−c), which indicates that all the above conditions are indispensable for the photocatalytic CO_2RR. Considering that **Ti_6−Fcdc** exhibits better photocatalytic performance than **Ti_6** and **Ti_8−Fcdc**, a series of control experiments with different solvent composition and a sacrificial electron donor have been carried out using **Ti_6−Fcdc** as an example. By these control experiments, we can systematically survey the significant influences of the above-mentioned conditions on photocatalytic CO_2RR and to determine the optimal conditions for photocatalytic CO_2RR (Table S7). Considering the energy band characteristics of **Ti_6−Fcdc**, we tried to perform photocatalytic CO_2RR in pure H_2O (without TIPA) (entry 2), and only trace amounts of $HCOO^-$ and CO are detected. Adjusting the ratio of the solvent, a small amount of $HCOO^-$ and trace amounts of CO are detected under the conditions of H_2O/TIPA= 14/1 (entry 3). While TIPA is replaced with another sacrificial agent TEOA (entry 4), only trace amounts of $HCOO^-$ are detected. Using acetonitrile as the solvent for photocatalytic CO_2RR (entry 5), a small amount of $HCOO^-$ is detected. Trace amounts of $HCOO^-$ and CO are detected in the mixed solvent of H_2O and acetonitrile (entry 6). It can be confirmed that these three PTCs can photoreduce CO_2 to $HCOO^-$ under visible light, and Fcdc-functionalized **Ti_8−Fcdc** and **Ti_6−Fcdc** have higher photocatalytic performance. This further indicates that the successful introduction of Fcdc ligand has improved the photoreduction activity of PTCs. For comparison, we list the photocatalytic properties of a range of reported crystalline materials for visible light-irradiated reducing CO_2 to $HCOO^-$ (Table S8).

The liquid phase UV−vis absorption test of the solutions after the photocatalytic reaction of **Ti_6**, **Ti_8−Fcdc**, and **Ti_6−Fcdc** is further performed. The results reveal that the liquid phase UV−vis absorption spectrum of **Ti_6**, **Ti_8−Fcdc**, and **Ti_6−Fcdc** are basically the same as those before the reaction (Figures S38−S40). To verify the stability of these PTCs, the solutions of photocatalytic reaction have been detected by the Raman spectroscopy (Figures S41−S43). The results showed that the liquid phase Raman spectra of **Ti_6**, **Ti_8−Fcdc**, and **Ti_6−Fcdc** are basically the same as those before the reaction, which eliminates the effect of the active components decomposed break away from the photocatalyst on the photocatalytic activity. At the same time, the solution stability behavior of the representative **Ti_6−Fcdc** cluster for photocatalytic reaction is examined by high-resolution mass spectroscopy (HR−MS) (Figures S44 and S45). The analytical results displayed that the fragment peaks of the catalyst

https://doi.org/10.1021/acscatal.0c04495
ACS Catal. 2021, 11, 4510−4519

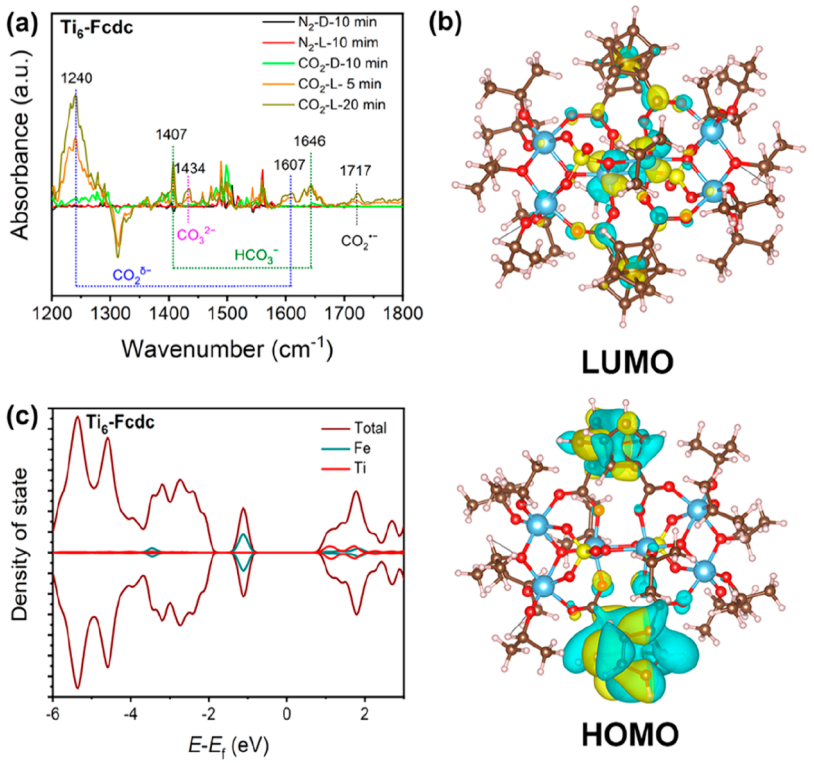

Figure 4. (a) In situ FTIR spectra on **Ti_6−Fcdc**. (b) The LUMO and HOMO orbitals calculated for **Ti_6−Fcdc**. (c) DOS plots of **Ti_6−Fcdc**. E_f refers to "Fermi level" that is the center between HOMO and LUMO.

molecule structure before and after the reaction are consistent. In short, these results demonstrated that Fcdc-functionalized **Ti_8−Fcdc** and **Ti_6−Fcdc** can actually serve as stable and efficient photocatalyst in CO_2RR.

Furthermore, we verified the photocatalytic CO_2RR mechanism of these PTCs through electron paramagnetic spin resonance spectroscopy (ESR) measurements (Figure S46 and S47). The results exhibited that the reaction system including the sample and the sacrificial agent did not show any ESR signal in N_2 atmosphere without light irradiation. The obvious signal of Ti^{3+} ions in **Ti_8−Fcdc** and **Ti_6−Fcdc** could be noticed from the ESR spectrum under visible light irradiation, corresponding to g = 1.945 and g = 1.947, respectively.[50] This implies that the Fcdc ligand within the **Ti_8−Fcdc** and **Ti_6−Fcdc** transfers photoexcited electrons to the Ti^{4+} ions, and then Ti^{4+} ions are reduced to Ti^{3+} ions. Meanwhile, TIPA is used to be sacrificial agents to offset the photogenerated holes. Besides, the signal of the Ti^{3+} ions gradually become prominent as the irradiation time prolonged. While the reaction system is in contact with the CO_2 atmosphere, the ESR signal of Ti^{3+} ions gradually disappears, which indicated that the photogenerated Ti^{3+} ions are involved in the CO_2RR. ESR results show that the Ti^{4+} ions within the Fcdc functionalized **Ti_8−Fcdc** and **Ti_6−Fcdc** act as the active centers for photocatalytic CO_2RR.

To probe the CO_2 radical and other reaction intermediates in the photocatalytic reaction, the Fcdc functionalized **Ti_6−Fcdc** is investigated by in situ Fourier transform infrared (FTIR) spectroscopy. In the in situ FTIR spectra of **Ti_6−Fcdc**, under dark conditions in N_2 or CO_2 atmosphere and under irradiation for 10 min in N_2 atmosphere, no significant changes in vibrational peaks are observed (Figure 4a). In contrast, the peaks at 1240, 1407, 1434, 1607, 1646, and 1717 cm^{-1} obviously appear after exposure to CO_2 atmosphere for 5 min. As we have noticed in Figure 4a, the signal appeared at 1717 cm^{-1}, and it gradually strengthened with the increase of the irradiation time. This can be ascribed to the CO_2 radical, which is one of the essential intermediates for photoreduction of CO_2-to-$HCOO^-$.[56] Meanwhile, the peaks appearing at 1240 and 1607 cm^{-1} mean the formation of carboxylate ($CO_2^{\delta-}$),[57] the features at 1407 and 1646 cm^{-1} are attributed to the formation of bicarbonates,[56,58] and the spectral band at 1343 cm^{-1} is carbonates.[57] When the irradiation time rose to 20 min, the peaks at 1240 and 1607 cm^{-1} enhanced with increasing time, while the peaks of bicarbonate at 1407 and 1646 cm^{-1} are essentially unchanged with increasing time, which may be attributed to the fact that carbonate can be present in large amounts in alkaline environments, which is consistent with the results of ^{13}C NMR.

In order to further understand the charge transfer properties of these functionalized polyoxo-titanium clusters, density functional theory (DFT) calculations are conducted for **Ti_6−Fcdc** and **Ti_6**, respectively. As shown in Figure 4b, for the Fcdc functionalized **Ti_6−Fcdc**, the electron density of HOMO orbitals is mostly concentrated on the Fe 3d orbital of the Fcdc ligand, along with some contribution from the π orbitals on the Fc rings, as observed for the {Ti_4} cluster and {Ti_6} cluster modified by ferrocene carboxylic acid.[44−46] The LUMO orbitals of **Ti_6−Fcdc** primarily lie on the Ti 3d orbital of the Ti-oxo nucleus. DFT calculation results indicate that the electron leap of the Fcdc functionalized polyoxo-titanium cluster is mainly the transition from the Fe 3d orbital in the Fcdc ligand to the Ti 3d orbital of the titanium-oxo nucleus. On the contrary, the electron density of the HOMO orbital of **Ti_6** is located at the O 2p orbital of the isopropanol molecule,[54] and its LUMO orbital is largely occupied by the

https://doi.org/10.1021/acscatal.0c04495
ACS Catal. 2021, 11, 4510−4519

Ti 3d orbital of the Ti-oxo nucleus (Figure S48). This result indicates that the electron transition of $\mathbf{Ti_6}$ is mainly from the charge transfer of O 2p → Ti 3d. Furthermore, via the electronic structure analysis, it is found that Ti atoms contributed most of the total density of state (DOS) at the bottom of the "LUMO" (from E_f to E_f + 2.5 eV), for both $\mathbf{Ti_6}$−**Fcdc** and $\mathbf{Ti_6}$ (Figures 4c and S49). Whereas, the proportion of Ti atom in total DOS is much smaller in $\mathbf{Ti_6}$−**Fcdc**, as shown in Figure 4c. This suggested that the LUMO orbitals of $\mathbf{Ti_6}$−**Fcdc** is more delocalized. Considering photocatalytic CO_2RR only takes place at the positions where excited electron can possibly occur, such delocalized LUMO abandons the active sites, thus enhancing the activity of CO_2 photoreduction. This further indicates that the introduction of the Fcdc ligand enhances the charge transfer efficiency within the molecules of $\mathbf{Ti_8}$−**Fcdc** and $\mathbf{Ti_6}$−**Fcdc**.

On the basis of the above data analysis, a reasonable mechanism can be suggested to explain the photocatalytic CO_2RR on these PTCs (Figure 5). First, many electron−hole

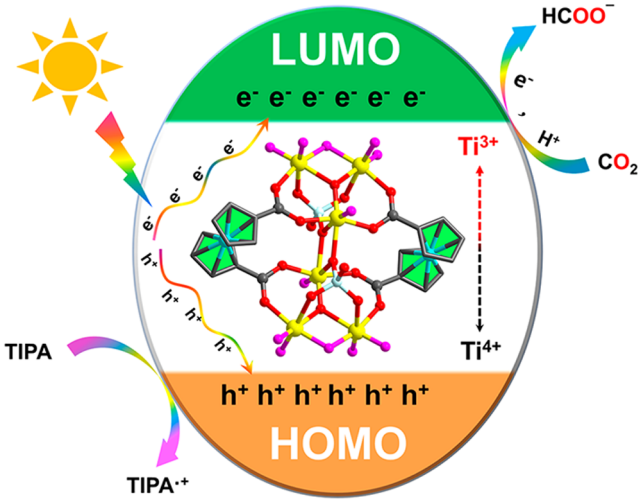

Figure 5. Plausible mechanism for photocatalytic CO_2RR over $\mathbf{Ti_6}$−**Fcdc** under visible-light irradiation.

pairs are generated in PTCs driven by visible light, and the Ti^{4+} ions in PTC obtain the photoexcited electrons migrated from the Fcdc ligands to become Ti^{3+} ions. At the same time, the TIPA molecules behave as sacrificial agents to quench the left photogenerated holes. At last, the accepted photoexcited electrons in Ti^{3+} ions further move to the absorbed CO_2 molecules for CO_2 reduction reaction, while Ti^{3+} ions are oxidized to the original Ti^{4+} ions. On this foundation, under the conditions of H_2O and TIPA (electron and proton donor), $\mathbf{Ti_6}$, $\mathbf{Ti_8}$−**Fcdc**, and $\mathbf{Ti_6}$−**Fcdc** can achieve a complete CO_2-to-$HCOO^-$ photosynthetic cycle. The above experimental results are consistent with our previously reported mechanism of PTC-based photocatalyst for CO_2RR.[34,35] Notably, the introduction of Fcdc ligand into $\mathbf{Ti_8}$−**Fcdc** and $\mathbf{Ti_6}$−**Fcdc** greatly expands the light absorption region, and accelerates the effective electron transfer rate, thereby raising the photocatalytic performance of PTCs.

CONCLUSIONS

In summary, we have successfully constructed three different PTC-based photocatalysts for the photocatalytic CO_2RR, which are $\mathbf{Ti_6}$ and the Fcdc functionalized $\mathbf{Ti_8}$−**Fcdc** and $\mathbf{Ti_6}$−**Fcdc**. Owing to the introduction of Fcdc ligands, the light absorption range of Fcdc functionalized $\mathbf{Ti_8}$−**Fcdc** and $\mathbf{Ti_6}$−**Fcdc** extends to the visible light region. Compared with $\mathbf{Ti_6}$ without Fcdc ligand coordination, the successful introduction of Fcdc ligand effectively enhanced the charge transfer within the $\mathbf{Ti_8}$−**Fcdc** and $\mathbf{Ti_6}$−**Fcdc** structure. On the basis of these advantages, $\mathbf{Ti_6}$, $\mathbf{Ti_8}$−**Fcdc**, and $\mathbf{Ti_6}$−**Fcdc** acted as photocatalysts to conduct photocatalytic CO_2RR in water containing TIPA under visible light. The Fcdc functionalized $\mathbf{Ti_8}$−**Fcdc** and $\mathbf{Ti_6}$−**Fcdc** have superior catalytic performance for CO_2-to-$HCOO^-$ photosynthesis. Most importantly, the visible light-triggered catalytic performance of $\mathbf{Ti_6}$−**Fcdc** is the highest among the reported PTC catalyst systems for CO_2RR photoconversion in water. Our work represents an important case study for reasonably designing more specifically functionalized PTC-based photocatalysts to accomplish efficient CO_2RR.

ASSOCIATED CONTENT

Supporting Information

The Supporting Information is available free of charge at https://pubs.acs.org/doi/10.1021/acscatal.0c04495.

Crystallographic data for $\mathbf{Ti_8}$−**Fcdc** (CIF)

Crystallographic data for $\mathbf{Ti_6}$−**Fcdc** (CIF)

Details of photocatalytical measurement, more characterizations, and DFT calculation (PDF)

AUTHOR INFORMATION

Corresponding Authors

Jiang Liu − *School of Chemistry and Materials Science, Nanjing Normal University, Nanjing 210023, P. R. China*; Email: liuj@njnu.edu.cn

Shun-Li Li − *School of Chemistry and Materials Science, Nanjing Normal University, Nanjing 210023, P. R. China*; Email: slli@njnu.edu.cn

Ya-Qian Lan − *School of Chemistry and Materials Science, Nanjing Normal University, Nanjing 210023, P. R. China*; orcid.org/0000-0002-2140-7980; Email: yqlan@njnu.edu.cn

Authors

Jing-Jing Liu − *School of Chemistry and Materials Science, Nanjing Normal University, Nanjing 210023, P. R. China*

Ning Li − *School of Chemistry and Chemical Engineering, Yangzhou University, Yangzhou 225002, P. R. China*

Jia-Wei Sun − *School of Chemistry and Materials Science, Nanjing Normal University, Nanjing 210023, P. R. China*

Long-Zhang Dong − *School of Chemistry and Materials Science, Nanjing Normal University, Nanjing 210023, P. R. China*; orcid.org/0000-0002-9276-5101

Su-Juan Yao − *School of Chemistry and Materials Science, Nanjing Normal University, Nanjing 210023, P. R. China*

Lei Zhang − *School of Chemistry and Materials Science, Nanjing Normal University, Nanjing 210023, P. R. China*

Zhi-Feng Xin − *Institute of Molecular Engineering and Applied Chemistry, Anhui University of Technology, Ma'anshan, Anhui 243002, P. R. China*

Jing-Wen Shi − *Henan Key Laboratory of Polyoxometalate Chemistry, College of Chemistry and Chemical, Engineering, Henan University, Kaifeng, Henan 475004, P. R. China*

Jing-Xuan Wang − *School of Chemistry and Materials Science, Nanjing Normal University, Nanjing 210023, P. R. China*

https://doi.org/10.1021/acscatal.0c04495
ACS Catal. 2021, 11, 4510−4519

Complete contact information is available at:
https://pubs.acs.org/10.1021/acscatal.0c04495

Author Contributions

Y.-Q.L., S.-L.L., J.L., and J.-J.L. conceived and designed the idea; J.-J.L., J.-W.S., and J.-X.W. prepared the experimental materials. J.-J.L., L.-Z.D., S.-J.Y. and N.L. conducted the characterizations and designed the photocatalytic CO_2 reduction reaction. L.Z., Z.-F.X., and J.-W.S. collected and analyzed the data. J.-J.L. discussed the results and prepared the manuscript. All the authors reviewed and contributed to this paper.

Notes

The authors declare no competing financial interest.

■ ACKNOWLEDGMENTS

This work was financially supported by the NSFC (No. 21622104, 92061101, 21871142, and 21901122); the NSF of Jiangsu Province of China (No. BK20171032); Natural Science Research of Jiangsu Higher Education Institutions of China (No. 19KJB150011), the Project funded by the China Postdoctoral Science Foundation (No. 2018M630572 and 2019M651873), the Priority Academic Program Development of Jiangsu Higher Education Institutions, and the Foundation of Jiangsu Collaborative Innovation Center of Biomedical Functional Materials.

■ REFERENCES

(1) Sanz-Pérez, E. S.; Murdock, C. R.; Didas, S. A.; Jones, C. W. Direct Capture of CO_2 from Ambient Air. *Chem. Rev.* **2016**, *116*, 11840−11876.
(2) Bo, Y.; Gao, C.; Xiong, Y. Recent advances in engineering active sites for photocatalytic CO_2 reduction. *Nanoscale* **2020**, *12*, 12196−12209.
(3) Goeppert, A.; Czaun, M.; Jones, J.-P.; Surya Prakash, G. K.; Olah, G. A. Recycling of carbon dioxide to methanol and derived products - closing the loop. *Chem. Soc. Rev.* **2014**, *43*, 7995−8048.
(4) Steinlechner, C.; Junge, H. Renewable Methane Generation from Carbon Dioxide and Sunlight. *Angew. Chem., Int. Ed.* **2018**, *57*, 44−45.
(5) Davis, S. J.; Caldeira, K.; Matthews, H. D. Future CO_2 Emissions and Climate Change from Existing Energy Infrastructure. *Science* **2010**, *329*, 1330.
(6) Xiong, X.; Zhao, Y.; Shi, R.; Yin, W.; Zhao, Y.; Waterhouse, G. I. N.; Zhang, T. Selective photocatalytic CO_2 reduction over Zn-based layered double hydroxides containing tri or tetravalent metals. *Science Bulletin* **2020**, *65*, 987−994.
(7) Chen, G.; Waterhouse, G. I. N.; Shi, R.; Zhao, J.; Li, Z.; Wu, L.-Z.; Tung, C.-H.; Zhang, T. From Solar Energy to Fuels: Recent Advances in Light-Driven C1 Chemistry. *Angew. Chem., Int. Ed.* **2019**, *58*, 17528−17551.
(8) Li, K.; Peng, B.; Peng, T. Recent Advances in Heterogeneous Photocatalytic CO_2 Conversion to Solar Fuels. *ACS Catal.* **2016**, *6*, 7485−7527.
(9) Li, N.; Liu, J.; Liu, J.-J.; Dong, L.-Z.; Xin, Z.-F.; Teng, Y.-L.; Lan, Y.-Q. Adenine Components in Biomimetic Metal-Organic Frameworks for Efficient CO_2 Photoconversion. *Angew. Chem., Int. Ed.* **2019**, *58*, 5226−5231.
(10) Zhang, M.; Lu, M.; Lang, Z.-L.; Liu, J.; Liu, M.; Chang, J.-N.; Li, L.-Y.; Shang, L.-J.; Wang, M.; Li, S.-L.; Lan, Y.-Q. Semiconductor/Covalent-Organic-Framework Z-Scheme Heterojunctions for Artificial Photosynthesis. *Angew. Chem., Int. Ed.* **2020**, *59*, 6500−6506.
(11) Xu, H. Q.; Hu, J.; Wang, D.; Li, Z.; Zhang, Q.; Luo, Y.; Yu, S. H.; Jiang, H. L. Visible-Light Photoreduction of CO_2 in a Metal-Organic Framework: Boosting Electron-Hole Separation via Electron Trap States. *J. Am. Chem. Soc.* **2015**, *137*, 13440−13443.
(12) Dong, L.-Z.; Zhang, L.; Liu, J.; Huang, Q.; Lu, M.; Ji, W.-X.; Lan, Y.-Q. Stable Heterometallic Cluster-Based Organic Framework Catalysts for Artificial Photosynthesis. *Angew. Chem., Int. Ed.* **2020**, *59*, 2659−2663.
(13) Tu, W.; Zhou, Y.; Zou, Z. Photocatalytic Conversion of CO_2 into Renewable Hydrocarbon Fuels: State-of-the-Art Accomplishment, Challenges, and Prospects. *Adv. Mater.* **2014**, *26*, 4607−4626.
(14) Yan, Z. H.; Du, M. H.; Liu, J.; Jin, S.; Wang, C.; Zhuang, G. L.; Kong, X. J.; Long, L. S.; Zheng, L. S. Photo-generated dinuclear $\{Eu(II)\}_2$ active sites for selective CO_2 reduction in a photosensitizing metal-organic framework. *Nat. Commun.* **2018**, *9*, 3353.
(15) Zhang, H.; Liu, G.; Shi, L.; Liu, H.; Wang, T.; Ye, J. Engineering coordination polymers for photocatalysis. *Nano Energy* **2016**, *22*, 149−168.
(16) Xie, S.-L.; Liu, J.; Dong, L.-Z.; Li, S.-L.; Lan, Y.-Q.; Su, Z.-M. Hetero-metallic active sites coupled with strongly reductive polyoxometalate for selective photocatalytic CO_2-to-CH_4 conversion in water. *Chem. Sci.* **2019**, *10*, 185−190.
(17) Lin, J.; Pan, Z.; Wang, X. Photochemical Reduction of CO_2 by Graphitic Carbon Nitride Polymers. *ACS Sustainable Chem. Eng.* **2014**, *2*, 353−358.
(18) Zhou, B.; Song, J.; Xie, C.; Chen, C.; Qian, Q.; Han, B. Mo-Bi-Cd Ternary Metal Chalcogenides: Highly Efficient Photocatalyst for CO_2 Reduction to Formic Acid Under Visible Light. *ACS Sustainable Chem. Eng.* **2018**, *6*, 5754−5759.
(19) Wang, Y.; Huang, N. Y.; Shen, J. Q.; Liao, P. Q.; Chen, X. M.; Zhang, J. P. Hydroxide Ligands Cooperate with Catalytic Centers in Metal-Organic Frameworks for Efficient Photocatalytic CO_2 Reduction. *J. Am. Chem. Soc.* **2018**, *140*, 38−41.
(20) Wang, L.; Jin, P.; Duan, S.; She, H.; Huang, J.; Wang, Q. In-situ incorporation of Copper(II) porphyrin functionalized zirconium MOF and TiO_2 for efficient photocatalytic CO_2 reduction. *Science Bulletin* **2019**, *64*, 926−933.
(21) Fu, J.; Yu, J.; Jiang, C.; Cheng, B. g-C_3N_4-Based Heterostructured Photocatalysts. *Adv. Energy Mater.* **2018**, *8*, 1701503.
(22) Kim, D.; Sakimoto, K. K.; Hong, D.; Yang, P. Artificial photosynthesis for sustainable fuel and chemical production. *Angew. Chem., Int. Ed.* **2015**, *54*, 3259−3266.
(23) Rao, H.; Schmidt, L. C.; Bonin, J.; Robert, M. Visible-light-driven methane formation from CO_2 with a molecular iron catalyst. *Nature* **2017**, *548*, 74−77.
(24) Zhao, Y.; Chen, G.; Bian, T.; Zhou, C.; Waterhouse, G. I.; Wu, L. Z.; Tung, C. H.; Smith, L. J.; O'Hare, D.; Zhang, T. Defect-Rich Ultrathin ZnAl-Layered Double Hydroxide Nanosheets for Efficient Photoreduction of CO_2 to CO with Water. *Adv. Mater.* **2015**, *27*, 7824−7831.
(25) Schneider, J.; Matsuoka, M.; Takeuchi, M.; Zhang, J.; Horiuchi, Y.; Anpo, M.; Bahnemann, D. W. Understanding TiO_2 Photocatalysis: Mechanisms and Materials. *Chem. Rev.* **2014**, *114*, 9919−9986.
(26) Kumaravel, V.; Mathew, S.; Bartlett, J.; Pillai, S. C. Photocatalytic hydrogen production using metal doped TiO_2: A review of recent advances. *Appl. Catal., B* **2019**, *244*, 1021−1064.
(27) Zhang, J.; Xu, Q.; Feng, Z.; Li, M.; Li, C. Importance of the relationship between surface phases and photocatalytic activity of TiO_2. *Angew. Chem., Int. Ed.* **2008**, *47*, 1766−1769.
(28) Tan, Y.-X.; Wang, F.; Zhang, J. Design and synthesis of multifunctional metal-organic zeolites. *Chem. Soc. Rev.* **2018**, *47*, 2130−2144.
(29) Coppens, P.; Chen, Y.; Trzop, E. Crystallography and Properties of Polyoxotitanate Nanoclusters. *Chem. Rev.* **2014**, *114*, 9645−9661.
(30) Liu, Y.-J.; Fang, W.-H.; Zhang, L.; Zhang, J. Recent advances in heterometallic polyoxotitanium clusters. *Coord. Chem. Rev.* **2020**, *404*, 213099.
(31) Rozes, L.; Sanchez, C. Titanium oxo-clusters: precursors for a Lego-like construction of nanostructured hybrid materials. *Chem. Soc. Rev.* **2011**, *40*, 1006−1030.

(32) Fan, X.; Wang, J.; Wu, K.; Zhang, L.; Zhang, J. Isomerism in Titanium-Oxo Clusters: Molecular Anatase Model with Atomic Structure and Improved Photocatalytic Activity. *Angew. Chem., Int. Ed.* **2019**, *58*, 1320−1323.
(33) Fang, W.-H.; Zhang, L.; Zhang, J. A 3.6 nm Ti_{52}-Oxo Nanocluster with Precise Atomic Structure. *J. Am. Chem. Soc.* **2016**, *138*, 7480−7483.
(34) Scanlon, D. O.; Dunnill, C. W.; Buckeridge, J.; Shevlin, S. A.; Logsdail, A. J.; Woodley, S. M.; Catlow, C. R.; Powell, M. J.; Palgrave, R. G.; Parkin, I. P.; Watson, G. W.; Keal, T. W.; Sherwood, P.; Walsh, A.; Sokol, A. A. Band alignment of rutile and anatase TiO_2. *Nat. Mater.* **2013**, *12*, 798−801.
(35) Jiang, Z.; Liu, J.; Gao, M.; Fan, X.; Zhang, L.; Zhang, J. Assembling Polyoxo-Titanium Clusters and CdS Nanoparticles to a Porous Matrix for Efficient and Tunable H_2-Evolution Activities with Visible Light. *Adv. Mater.* **2017**, *29*, 1603369.
(36) Su, K.; Wu, M.; Tan, Y.; Wang, W.; Yuan, D.; Hong, M. A monomeric bowl-like pyrogallol[4]arene Ti_{12} coordination complex. *Chem. Commun.* **2017**, *53*, 9598−9601.
(37) Li, N.; Liu, J.-J.; Sun, J.-W.; Dong, B.-X.; Dong, L.-Z.; Yao, S.-J.; Xin, Z.; Li, S.-L.; Lan, Y.-Q. Calix[8]arene-constructed stable polyoxotitanium clusters for efficient CO_2 photoreduction. *Green Chem.* **2020**, *22*, 5325−5332.
(38) Li, N.; Liu, J.; Liu, J. J.; Dong, L. Z.; Li, S. L.; Dong, B. X.; Kan, Y. H.; Lan, Y. Q. Self-Assembly of a Phosphate-Centered Polyoxo-Titanium Cluster: Discovery of the Heteroatom Keggin Family. *Angew. Chem., Int. Ed.* **2019**, *58*, 17260−17264.
(39) Fu, Y.; Sun, D.; Chen, Y.; Huang, R.; Ding, Z.; Fu, X.; Li, Z. An Amine-Functionalized Titanium Metal-Organic Framework Photocatalyst with Visible-Light-Induced Activity for CO_2 Reduction. *Angew. Chem., Int. Ed.* **2012**, *51*, 3364−3367.
(40) Hou, J.-L.; Weng, Y.-G.; Liu, P.-Y.; Cui, L.-N.; Zhu, Q.-Y.; Dai, J. Effects of the Ligand Structures on the Photoelectric Activities, a Model Study Based on Titanium-Oxo Clusters Anchored with S-Heterocyclic Ligands. *Inorg. Chem.* **2019**, *58*, 2736−2743.
(41) Gao, M.-Y.; Fang, W.-H.; Wen, T.; Zhang, L.; Zhang, J. Connecting Titanium-Oxo Clusters by Nitrogen Heterocyclic Ligands to Produce Multiple Cluster Series with Photocatalytic H_2 Evolution Activities. *Cryst. Growth Des.* **2017**, *17*, 3592−3595.
(42) Liu, J.-X.; Gao, M.-Y.; Fang, W.-H.; Zhang, L.; Zhang, J. Bandgap Engineering of Titanium-Oxo Clusters: Labile Surface Sites Used for Ligand Substitution and Metal Incorporation. *Angew. Chem., Int. Ed.* **2016**, *55*, 5160−5165.
(43) Jäkle, F.; Sheridan, J. B. Ferrocenes. Ligands, Materials and Biomolecules. Edited by Petr Štěpnička. *Angew. Chem., Int. Ed.* **2008**, *47* (40), 7587−7587.
(44) Singh, S. K.; Chauhan, R.; Singh, B.; Diwan, K.; Kociok-Köhn, G.; Bahadur, L.; Singh, N. Enhanced light harvesting efficiencies of bis(ferrocenylmethyl)-based sulfur rich sensitizers used in dye sensitized TiO_2 solar cells. *Dalton Trans.* **2012**, *41*, 1373−1380.
(45) Liu, Z.; Lei, J.; Frasconi, M.; Li, X.; Cao, D.; Zhu, Z.; Schneebeli, S. T.; Schatz, G. C.; Stoddart, J. F. A square-planar tetracoordinate oxygen-containing Ti_4O_{17} cluster stabilized by two 1,1′-ferrocenedicarboxylato ligands. *Angew. Chem., Int. Ed.* **2014**, *53*, 9193−9197.
(46) Fan, Y.; Li, H.-M.; Duan, R.-H.; Lu, H.-T.; Cao, J.-T.; Zou, G.-D.; Jing, Q.-S. Phosphonate-Stabilized Titanium-Oxo Clusters with Ferrocene Photosensitizer: Structures, Photophysical and Photoelectrochemical Properties, and DFT/TDDFT Calculations. *Inorg. Chem.* **2017**, *56*, 12775−12782.
(47) Hou, J.-L.; Huo, P.; Tang, Z.-Z.; Cui, L.-N.; Zhu, Q.-Y.; Dai, J. A Titanium Oxo Cluster Model Study of Synergistic Effect of Co-coordinated Dye Ligands on Photocurrent Responses. *Inorg. Chem.* **2018**, *57*, 7420−7427.
(48) Fan, Y.; Cui, Y.; Zou, G.-D.; Duan, R.-H.; Zhang, X.; Dong, Y.-X.; Lv, H.-T.; Cao, J.-T.; Jing, Q.-S. A ferrocenecarboxylate-functionalized titanium-oxo-cluster: the ferrocene wheel as a sensitizer for photocurrent response. *Dalton Trans.* **2017**, *46*, 8057−8064.
(49) Hou, J.-L.; Luo, W.; Guo, Y.; Zhang, P.; Yang, S.; Zhu, Q.-Y.; Dai, J. Titanium Oxo Cluster with Six Peripheral Ferrocene Units and Its Photocurrent Response Properties for Saccharides. *Inorg. Chem.* **2017**, *56*, 6451−6458.
(50) He, Y.-P.; Yuan, L.-B.; Chen, G.-H.; Lin, Q.-P.; Wang, F.; Zhang, L.; Zhang, J. Water-Soluble and Ultrastable Ti_4L_6 Tetrahedron with Coordination Assembly Function. *J. Am. Chem. Soc.* **2017**, *139*, 16845−16851.
(51) Turlington, M. D.; Pienkos, J. A.; Carlton, E. S.; Wroblewski, K. N.; Myers, A. R.; Trindle, C. O.; Altun, Z.; Rack, J. J.; Wagenknecht, P. S. Complexes with Tunable Intramolecular Ferrocene to Ti^{IV} Electronic Transitions: Models for Solid State Fe^{II} to Ti^{IV} Charge Transfer. *Inorg. Chem.* **2016**, *55*, 2200−2211.
(52) Li, X.-X.; Liu, J.; Zhang, L.; Dong, L.-Z.; Xin, Z.-F.; Li, S.-L.; Huang-Fu, X.-Q.; Huang, K.; Lan, Y.-Q. Hydrophobic Polyoxometalate-Based Metal-Organic Framework for Efficient CO_2 Photoconversion. *ACS Appl. Mater. Interfaces* **2019**, *11*, 25790−25795.
(53) Melchionna, M.; Fornasiero, P. Updates on the Roadmap for Photocatalysis. *ACS Catal.* **2020**, *10*, 5493−5501.
(54) Lv, H.-T.; Li, H.-M.; Zou, G.-D.; Cui, Y.; Huang, Y.; Fan, Y. Titanium-oxo clusters functionalized with catecholate-type ligands: modulating the optical properties through charge-transfer transitions. *Dalton Trans.* **2018**, *47*, 8158−8163.
(55) Fu, J.; Jiang, K.; Qiu, X.; Yu, J.; Liu, M. Product selectivity of photocatalytic CO_2 reduction reactions. *Mater. Today* **2020**, *32*, 222−243.
(56) Zu, X.; Li, X.; Liu, W.; Sun, Y.; Xu, J.; Yao, T.; Yan, W.; Gao, S.; Wang, C.; Wei, S.; Xie, Y. Efficient and Robust Carbon Dioxide Electroreduction Enabled by Atomically Dispersed $Sn^{\delta+}$ Sites. *Adv. Mater.* **2019**, *31*, 1808135.
(57) Wang, L.; Guan, E.; Wang, Y.; Wang, L.; Gong, Z.; Cui, Y.; Meng, X.; Gates, B. C.; Xiao, F.-S. Silica accelerates the selective hydrogenation of CO_2 to methanol on cobalt catalysts. *Nat. Commun.* **2020**, *11*, 1033.
(58) Bando, K. K.; Sayama, K.; Kusama, H.; Okabe, K.; Arakawa, H. J. A. C. A.-G. In-situ FT-IR study on CO_2 hydrogenation over Cu catalysts supported on SiO_2, Al_2O_3, and TiO_2. *Appl. Catal., A* **1997**, *165*, 391−409.

https://doi.org/10.1021/acscatal.0c04495
ACS Catal. 2021, 11, 4510−4519